



HAL
open science

Revisiting the Taylor-Culick approximation. Part 2: retraction of a viscous sheet

Hiranya Deka, Jean-Lou Pierson

► **To cite this version:**

Hiranya Deka, Jean-Lou Pierson. Revisiting the Taylor-Culick approximation. Part 2 : retraction of a viscous sheet. *Physical Review Fluids*, 2020, 5 (9), 10.1103/PhysRevFluids.5.093603 . hal-03002192

HAL Id: hal-03002192

<https://ifp.hal.science/hal-03002192>

Submitted on 12 Nov 2020

HAL is a multi-disciplinary open access archive for the deposit and dissemination of scientific research documents, whether they are published or not. The documents may come from teaching and research institutions in France or abroad, or from public or private research centers.

L'archive ouverte pluridisciplinaire **HAL**, est destinée au dépôt et à la diffusion de documents scientifiques de niveau recherche, publiés ou non, émanant des établissements d'enseignement et de recherche français ou étrangers, des laboratoires publics ou privés.

Revisiting the Taylor-Culick approximation. Part 2 : retraction of a viscous sheet

Hiranya Deka and Jean-Lou Pierson*

IFP Energies Nouvelles, Rond-point de l'changeur de Solaize, 69360 Solaize, France

(Dated: August 4, 2020)

Abstract

We study the retraction of a viscous liquid sheet of finite length with negligible effect of the ambient medium. Using the long-wavelength model we derive the scaling laws and similarity solution for the interface profile of the retracting sheet. Far from the tip, the similarity solution for the interface profiles converges to an asymptotic value of $1/4$. Direct numerical simulations are performed to compare the theoretical results with the simulations. When the inertia is negligible, the interface profiles remain flat during the retraction process which is in agreement with the self-similar solution. Using this similarity solution we derive the expression for the temporal variation of the tip speed for finite liquid sheets. We demonstrate that unlike an infinite sheet where the sheet retracts with a steady speed (known as Taylor-Culick speed), the tip speed decreases as a function of time for a finite liquid sheet. This is true when the viscous effects are larger than or of the same order with the inertia effects. Otherwise, the sheet retracts with the formation of a bulbous tip whose speed reaches a value closer to the Taylor-Culick speed.

I. Introduction

The retraction of liquid sheets has caught the attention of many researchers because of its importance in a variety of applications such as atomization [1–3] and coating [4–6]. The first theoretical investigation was performed by Dupré [7] where he reported that during the rupture of an inviscid soap film, the hole expands at a constant speed. Using energy balance, he derived the expression for the rim speed as $U = \sqrt{2\gamma/\rho h_0}$, where γ is the surface tension coefficient, ρ is the density of the soap film and h_0 is half of the initial thickness of the soap film. However, the experimental results obtained by Ranz [8] showed that the actual speed is less than that predicted by Dupré’s formula. Later on, Taylor [9] and Culick [10] independently showed that the speed of the rim is $1/\sqrt{2}$ smaller than that predicted by Dupré’s formula which was confirmed experimentally by McEntree & Mysels [11]. By balancing surface tension and inertia effects, and assuming that the liquid sheet retracts with the formation of a bulbous rim at its end, Taylor [9] and Culick [10] obtained the rim speed. This speed, also known as Taylor-Culick speed, is given as

$$U_{TC} = \sqrt{\frac{\gamma}{\rho h_0}}. \quad (1)$$

* jean-lou.pierson@ifpen.fr

Following that, many studies have been performed on the retraction of liquid sheets [6, 12–16]. The dynamics can be characterized in terms of the Ohnesorge number ($Oh = \mu/\sqrt{\rho\gamma h_0}$; μ is viscosity of the liquid sheet) which represents the relative importance of viscous and inertia-capillary forces. At low Ohnesorge number, the elongated sheet retracts with the formation of a bulbous rim which, after a transient stage, reaches the Taylor-Culick speed [6]. In the opposite regime of high Ohnesorge number, the film retracts with uniform thickening of the film without the formation of a bulbous end [14, 17]. Earlier numerical studies have shown that despite the change in geometry for high Ohnesorge number, for a sufficiently long sheet, the Taylor-Culick speed is reached in the long time limit [6, 14]. Murano and Okumura [16] recently studied experimentally the retraction of a liquid sheet formed by the bursting of a bubble at a free surface. In the high Ohnesorge number regime they found that the rim speed is better characterized by a balance between viscous and capillary effects rather than by Taylor-Culick speed. Thus, a natural question is what is the rim speed of a liquid sheet of finite length in the high Ohnesorge number regime.

In part 1 of this study [18] we have analyzed the retraction of an axisymmetric liquid ligament. We show that the Ohnesorge number has a dramatic influence on the retraction speed. In the present study, we focus on the viscous dominated regimes of 2D retracting sheets. To address this problem, we use a combination of theoretical arguments and numerical simulations. A long-wave model [19] for the retracting sheet is used to develop the theory. Based on the long-wave equations, we find a self-similar solution in the Stokes flow limit. Numerical simulations are also performed by solving the complete Navier-Stokes equations in order to examine the validity of the theoretical results. Two idealized configurations are simulated representing either the bursting of a soap film or a bursting bubble at a liquid-air interface. The rest of the paper is arranged as follows: first, we present our theoretical analysis, next we present the numerical results and discuss those results in comparison to the theory. Finally, we [wind up with a discussion and concluding remarks](#).

II. Theoretical analysis

A. Long-wave equations

A convenient and widely used theoretical model to study the retraction of a viscous sheet is the long-wave model. The long-wave equations are derived by Erneux and Davis [19] assuming that the elongated liquid sheet is slender $h_0 \ll L_0$ (h_0 is half of the initial

thickness of the liquid sheet and L_0 is half of its initial length) and the surrounding fluid has negligible effect on the flow dynamics. The long-wave equations for the motion of the slender liquid sheet can be written as [19, 20]

$$\frac{\partial h}{\partial t} + \frac{\partial(hu)}{\partial x} = 0 \quad (2)$$

$$\frac{\partial u}{\partial t} + u \frac{\partial u}{\partial x} = \frac{4\mu}{\rho h} \frac{\partial}{\partial x} \left(h \frac{\partial u}{\partial x} \right) - \frac{\gamma}{\rho} \frac{\partial \kappa}{\partial x} \quad (3)$$

Here, $h(x, t)$ is the half-thickness of the sheet; $u(x, t)$ is the x -directional velocity; t is time; μ is the dynamic viscosity and ρ is the density of the sheet liquid; γ is the surface tension coefficient. The curvature κ of the film is given by

$$\kappa = - \frac{\partial^2 h / \partial x^2}{(1 + (\partial h / \partial x)^2)^{3/2}}. \quad (4)$$

The complete expression for curvature is retained to capture the spherical cap at the tip of the retracting sheet. The same technique has been successfully used by many researchers [6, 14, 17].

Equation (3) is made dimensionless using the following scaling : $h = h_0 h^*$, $\kappa = (1/h_0) \kappa^*$, $z = L_0 z^*$, $t = (L_0/u_0) t^*$, $u = u_0 u^*$ where u_0 is a characteristic velocity which is a priori unknown. It gives

$$\frac{\rho h_0 u_0^2}{\gamma} \left(\frac{\partial u^*}{\partial t^*} + u^* \frac{\partial u^*}{\partial x^*} \right) = \frac{\mu u_0 h_0}{\gamma L_0} \frac{4}{h^*} \frac{\partial}{\partial x^*} \left(h^* \frac{\partial u^*}{\partial x^*} \right) - \frac{\partial \kappa^*}{\partial x^*} \quad (5)$$

By balancing surface tension effect and viscous effect we obtain the characteristic velocity $u_0 = (\gamma/\mu)L_0/h_0$ (hereafter the capillary velocity γ/μ and the capillary-viscous time scale $\mu h_0/\gamma$ are respectively written as U_v and t_v). Replacing u_0 , Eq. (5) can be rewritten as

$$\frac{(L_0/h_0)^2}{Oh^2} \left(\frac{\partial u^*}{\partial t^*} + u^* \frac{\partial u^*}{\partial x^*} \right) = \frac{4}{h^*} \frac{\partial}{\partial x^*} \left(h^* \frac{\partial u^*}{\partial x^*} \right) - \frac{\partial \kappa^*}{\partial x^*} \quad (6)$$

The inertial term becomes negligible if $Oh \gg L_0/h_0$. However, even at high Oh , the inertial term can be non-negligible if $Oh \sim L_0/h_0$. This scaling is similar to the one obtained in part 1 of this study [18] for an axisymmetric ligament.

B. Self-similar solution for $Oh \gg L_0/h_0$

In this study, we are interested in the retraction dynamics a liquid sheet for which the flow is governed by the viscous and the capillary forces. Following the analysis of Sec. II A,

we assume $Oh \gg L_0/h_0$ and we completely neglect the inertial term. Therefore, Eq. (3) can be written as

$$0 = \frac{4\mu}{h} \frac{\partial}{\partial x} \left(h \frac{\partial u}{\partial x} \right) - \gamma \frac{\partial \kappa}{\partial x}. \quad (7)$$

Integrating Eq. (7) from x to L , i.e. from an arbitrary position on the sheet to its tip

$$0 = \int_x^L \left(4\mu \frac{\partial}{\partial x} \left(h \frac{\partial u}{\partial x} \right) \right) dx - \int_x^L \left(\gamma h \frac{\partial \kappa}{\partial x} \right) dx. \quad (8)$$

After some algebra we get

$$\left[4\mu h \frac{\partial u}{\partial x} \right]_x^L - \left[\gamma \left(-\frac{hh''}{(1+h'^2)^{3/2}} - \frac{1}{(1+h'^2)^{1/2}} \right) \right]_x^L = 0 \quad (9)$$

To evaluate the integral we assume that the liquid sheet has a round end-tip. The assumptions lead to the following boundary conditions: $h(L, t) = 0$ and $\partial h/\partial x(L, t) = \infty$. Applying the above boundary conditions in Eq. (9) and neglecting the higher-order terms for the curvature we obtain

$$4 \frac{\partial u}{\partial x} + \frac{\gamma}{\mu h} = 0. \quad (10)$$

Equation (10) gives the evolution of the sheet far from the tip. We now assume that the sheet is sufficiently long to be considered as semi-infinite [such that the idealized problem is independent of the initial length of the sheet](#). Moreover, without the loss of generality, we set the location of the tip at $x = 0$. The only physical parameter that appears in Eq. (10) is γ/μ . The thickness of the sheet can be written as $h = h(x, t, \gamma/\mu, h_0)$ since we have assumed that the sheet is semi-infinite. Here, two of the governing parameters have independent dimension: γ/μ and t . Hence, by dimensional analysis [21] we get

$$h = \frac{\gamma}{\mu}(t + t_0)H \left(\frac{x}{(\gamma/\mu)(t + t_0)}, \frac{h_0}{(\gamma/\mu)(t + t_0)} \right) \quad (11)$$

where t_0 is a shift in time which has to be determined a posteriori from the initial condition. We assume that $h_0/(\gamma/\mu(t + t_0)) \ll 1$ [which requires that \$1 \ll t/t_v\$, i.e. that the solution we are seeking for becomes valid after a sufficiently long time](#). Hence we look for a self-similar solution written as

$$\eta = \frac{x}{(\gamma/\mu)(t + t_0)}; \quad h = \frac{\gamma}{\mu}(t + t_0)H(\eta); \quad u = \frac{\gamma}{\mu}U(\eta) \quad (12)$$

where η is the self-similar variable; H and U are self-similar functions. Now, inserting the self-similar variables in Eqs. (2) and (10) we get the following ordinary differential equations (the primes represent derivative w.r.t. self-similar variable η)

$$HU' + UH' + H - H'\eta = 0, \quad (13)$$

$$U'H + \frac{1}{4} = 0. \quad (14)$$

The above two equations can be combined to deduce a differential equation for H

$$H''(1 - 4H) = H'^2/H. \quad (15)$$

Equation (15) is similar to that evinced by Eggers [22] while studying the post-breakup of an axisymmetric thread. Although no analytical solution can be obtained from Eq. (15), it can be shown that far from the tip i.e. for $\eta \gg 1$, $H \sim 1/4$. This leading order solution can also be obtained from the solution evidenced by Munro and Lister [23] who studied an infinite retracting sheet stretched along its edge. Indeed, considering the longitudinal strain rate as zero in their Eq. (2.5) the self-similar thickness H reduces to $1/4$. Although the derivation presented in Munro and Lister [23] is different from the present one, they nicely complement each other.

Equation (12) predicts that far from the tip, the thickness of the sheet evolves as

$$h(x, t) = \frac{\gamma(t + t_0)}{\mu} = h_0 \left(1 + \frac{1}{4} \frac{t}{t_v} \right), \quad (16)$$

where we have used the initial condition $h(t = 0) = h_0$ to find the value of $t_0 = 4t_v$. Now using this similarity solution $H = 1/4$ in Eq. (14) we obtain $U = 2C - \eta$ where C is a constant. To understand the meaning of C we follow Eggers and Fontelos [24]. Integrating Eq. (13) from 0 to η we obtain

$$\int_0^\eta \left[\frac{\eta}{2} + HU - H\eta \right]' d\eta = \int_0^\eta \left[\frac{1}{2} - 2H \right] d\eta. \quad (17)$$

Inserting the asymptotic behavior $H = 1/4$, $U = 2C - \eta$ valid for large η and the boundary condition at the tip $H = 0$ at $\eta = 0$ we get

$$\frac{C}{2} = \int_0^\eta \left[\frac{1}{2} - 2H \right] d\eta \quad (18)$$

Eq. (18) can be rearranged as

$$\int_0^\eta 2H d\eta = \int_0^\eta \frac{1}{2} d\eta - \frac{1}{2} \int_0^C d\eta = \frac{1}{4} \int_C^\eta 2d\eta \quad (19)$$

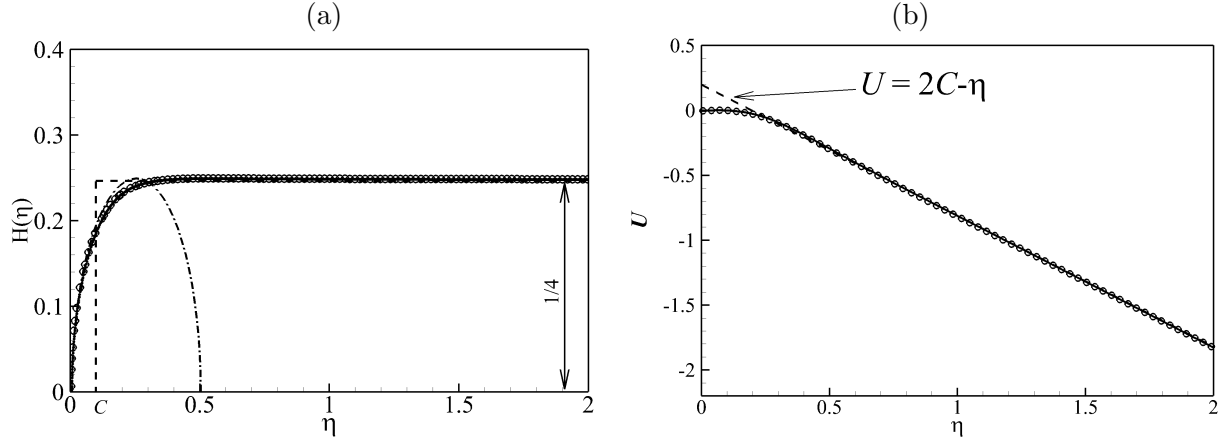


FIG. 1. (a) The self-similar interface profile and (b) the self-similar velocity profile. The numerical results for $L_0/h_0 = 10$ are shown by the solid line, while the circles are the results for $L_0/h_0 = 20$. The tip of the self-similar interface profile can be represented by a semi-circle with good accuracy (the dashed-dot line is a reference circle in (a)). In the velocity profile, the dashed line represents the theoretical solution $U = 2C - \eta$.

This implies that C is the tip position of a rectangle that has the same area as that of the liquid sheet.

The obtained similarity solutions for H and U are only valid far from the tip. To find the similarity solution valid everywhere we use numerical results. We have used the *Basilisk* solver [25–27] which solves the complete Navier-Stokes equations in the interior and exterior fluids. We have performed numerical simulations with two constant volume liquid sheets of initial aspect ratio 10 and 20. The similarity solutions obtained from the numerical simulation for $L_0/h_0 = 10$ and $L_0/h_0 = 20$ are shown in Fig. 1. In Fig. 1 (a), the retracting sheet profile is plotted in terms of the similarity variables H and η . There is no observable difference between the two cases considered here. Moreover, we plotted the results at different instant of time (larger than t_v) in terms of the self-similar variable H and η , and all the data collapsed on the same master curve. Hence, the sheets are sufficiently long to be considered as semi-infinite and represent well the self-similar solution. It is evident in Fig. 1 (a) that the similarity solution for H quickly reaches the a constant thickness $1/4$. The end shape of the similarity profile can be represented by a semi-circle with good accuracy (see Fig. 1 (a)). Figure 1 (b) shows the velocity profile within the liquid sheet in terms of the similarity variable U and η . A good agreement between the numerical simulations (circles and solid line) with the theoretical solution for the velocity profile $U = 2C - \eta$ (dashed line) corroborates the validity of the similarity solution. Fitting with the numerical data suggests that the value of the coefficient C is 0.0978 approximately.

III. Numerical results

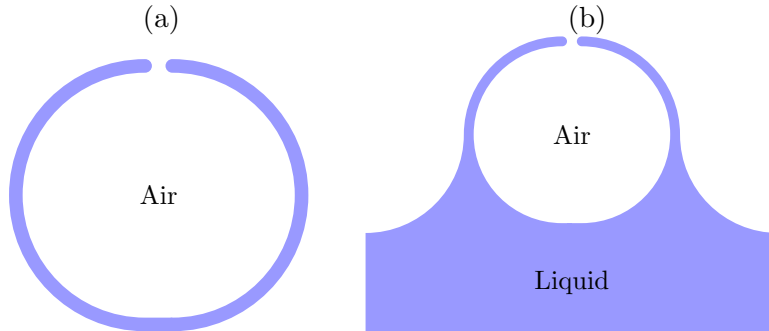


FIG. 2. (a) Schematic of a bursting soap film in air (midsection view), (b) Schematic of a bursting bubble at a liquid-air interface (midsection view).

Finite liquid sheets may appear in different practical situations such as rupture of a soap film [11] or bursting of a bubble at the surface of a pool [16]. These different cases encounter different boundary conditions far away from the tip. For example, during the bursting of a soap bubble in air (see Fig. 2 (a)), symmetry boundary condition can be observed at the axis of symmetry of the film. On the other hand, during the bursting of a bubble at a liquid-air interface (see Fig. 2 (b)), an outward flux of liquid is expected at the junction between the sheet and the pool. In this [section](#), we intend to study numerically the effect of each of these configurations on the retraction process. We consider simplified [versions of the aforementioned](#) configurations by neglecting the curvature of the sheet and considering [the geometry](#) as two-dimensional. Thus, the bursting of the soap film is investigated by considering the retraction of a symmetric 2D sheet while the bursting of the bubble is studied by assigning a pool at the end of a 2D sheet and joining the sheet and the pool by a large curvature region. The numerical details can be found in Refs. [18, 28] and typical script used to run the simulations can be found on the Basilisk website [27]. The results are discussed in different sections depending on the relative magnitude of Oh and L_0/h_0 as we observe different dynamics for different values of these parameters.

A. $Oh \gg L_0/h_0$

In this part, we consider $Oh \gg L_0/h_0$, i.e. the flow is controlled by the balance between the viscous and capillary forces, and the inertia of the fluid can be neglected.

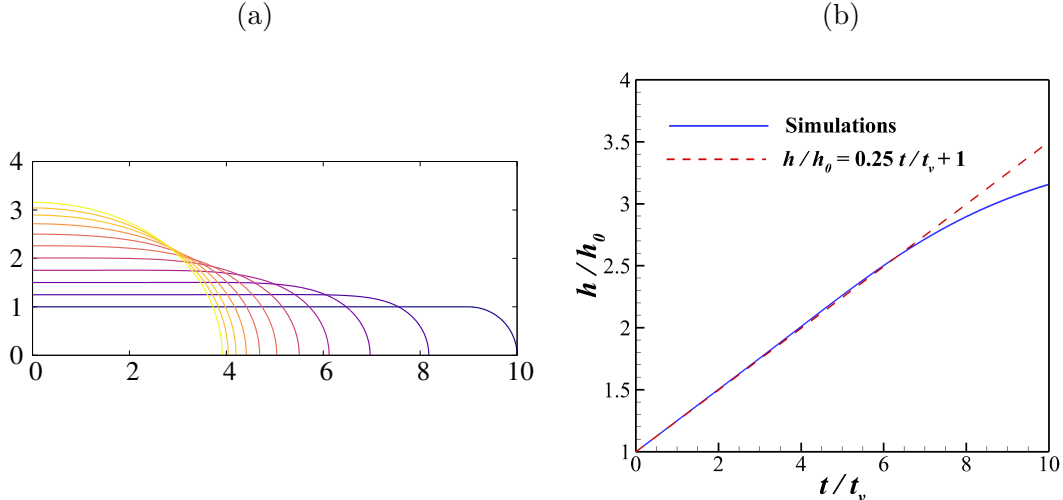


FIG. 3. (a) Interface profiles of the retracting sheet at different time instants. The profiles are plotted at time interval $\Delta t/t_v = 1$. (b) Temporal variation of the thickness of the sheet at $x = 0$. The dimensionless parameters are $Oh = 40$ and $L_0/h_0 = 10$.

1. *Bursting of a soap film*

The numerical results are in excellent agreement with the theory. This is evident in Fig. 3, which shows the temporal variation of the sheet thickness for the symmetry boundary condition mentioned above. The dimensionless parameters considered here are $Oh = 40$ and $L_0/h_0 = 10$. Figure 3 (a) shows the interface profiles of a retracting sheet at different time instants. The temporal variation of the thickness of the retracting sheet is presented in Fig. 3 (b) which shows that the thickness grows linearly with time in accordance with Eq. (16) or the self-similar solution discussed in Sec. II B. A deviation is seen in Fig. 3 (b) towards the later stage of retraction. Indeed, in the final stage of retraction, the length and the width of the sheet become comparable (or the tip region covers the whole domain) and the similarity solution is not valid. The self-similar solution is derived assuming that the liquid sheet is semi-infinite, which is not valid when the length and the width of the sheet become comparable. Nevertheless, the numerical simulations suggest that the similarity solution remains valid until the length of the sheet is approximately two times the thickness of the sheet.

A model for the retraction speed of the tip at the initial stage of the retraction has already been given by Savva and Bush [14]. They showed that the initial speed of the tip reads as $u_t = U_{TC} \sqrt{t/(\pi t_v)}$. This analytical result compares well with the numerical results for very short time $t \leq 0.01 t_v$ (Fig. 4 (a)). The agreement is even better for a larger aspect ratio.

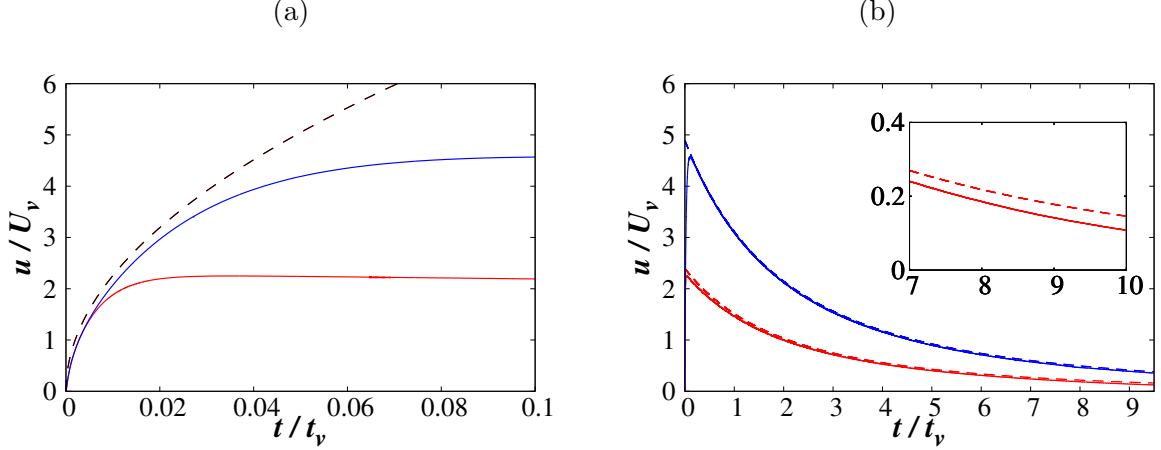


FIG. 4. Comparison of the retraction speed of the liquid sheet obtained from numerical simulations (solid lines) with the theoretical prediction (dashed lines). (a) The numerical results are compared with the early stage retraction theory of Savva and Bush [14]. (b) Comparison of the numerical results with the present theory (Eq. (20)) for the later stage of retraction. The results are shown for $Oh = 40, L_0/h_0 = 10$ (red color) and $Oh = 40, L_0/h_0 = 20$ (blue color). A zoomed view at the later stage when the self-similar solution is no longer valid is shown in the inner image for $Oh = 40, L_0/h_0 = 10$.

In a longer time, a noticeable deviation of the theory from the simulation is observed. It can be seen in Fig. 4 (a) that the speed of the tip (for both aspect ratios considered here) quickly reached a peak value while the theoretical model predicts a monotonic increase of the speed. This deviation from the theoretical model implies that the initial acceleration stage is over and the self-similar solution has become valid. Indeed the self-similar solution is supposed to be valid at $t/t_v \gg 1$.

Based on the self-similar solution, we now build a model for the speed of the tip. We assume that the sheet is rectangular with a semi-circular tip. The volume of the liquid sheet is constant and is equal to $V_0 = (L - h)2h + \pi h^2/2$ and hence, we have $L = V_0/2h + (1 - \pi/4)h$. Replacing h using Eq. (16) we obtain

$$\frac{dL}{dt} = U_v \left(-\frac{4(L_0/h_0 - 1) + \pi}{(t/t_v + 4)^2} + \frac{1}{4} \left(1 - \frac{\pi}{4} \right) \right) \quad (20)$$

where $-dL/dt$ is the tip speed. Remarkably, Eq. (20) shows that the slender liquid sheet does not retract at a steady speed. Indeed, the retraction speed of a finite liquid sheet decreases as a square of time. Moreover, the retraction speed in this regime is independent of the Ohnesorge number. The maximum speed scales linearly with the aspect ratio. Indeed, in the case of large aspect ratio ($L_0/h_0 \gg 1$) the maximum speed (at $t = 0$) scales as $0.25(L_0/h_0)U_v$.

Figure 4 (b) shows the comparison of the present long time asymptotic theory (Eq. (20)) with the numerical result. As evident in Fig. 4 (b), the numerical results are in very good agreement with the theoretical results corroborating that the speed of the retracting sheet is inversely proportional to the square of the time of retraction. The same level of agreement has been observed for the other values of dimensionless parameters (for example $Oh = 10, 20$) which are not repeated here. Moreover, the maximum speed reached by the tip scales linearly with the aspect ratio as predicted by the theory. At the later stage when the length and width of the sheet become comparable, the self-similar solution is no longer valid and the numerical results deviate a little from the theory although this deviation is not very significant. This deviation can be seen in the zoomed inner image of Fig. 4 (b).

2. *Bursting of a bubble at a liquid-air interface*

Next, we simulate the retraction of a liquid sheet attached to a pool. Fig. 5 (a) shows the interface profiles of the sheet when the other end of the sheet is connected to a pool. A circular arc of radius $5h_0$ is defined to match the planar pool and the sheet. Since the curvature of this region is large in comparison with the curvature of the tip, capillary effects are expected to be smaller. Hence the motion in this region is less pronounced in comparison with the sheet as evidenced in figure 5 (a). Remarkably, the sheet retracts with a uniform increase in thickness which suggests that the self-similar solution is valid. A zoomed view of the interfaces of the sheet at different time instants are shown in Fig. 5 (b). The temporal variation of the sheet thickness is plotted in Fig. 5 (c) which shows that the sheet thickness increases linearly with time with a slope $1/4$ in accordance with that predicted by the self-similar solution. As evinced in the previous section, we observe the same deviation in the temporal variation of sheet thickness with the theory in the long time limit due to the limitation of the self-similar solution when the aspect ratio reaches a value close to 2.

The short time asymptotic theory of Savva and Bush [14] is in good agreement with the numerical results (see Fig. 6) for the early stage of retraction. We observe that the time at which the numerical predictions deviate from the short time asymptotic theory is larger than the symmetric film studied in the last section. As a consequence, for the same dimensionless parameters, the maximum speed reached by the tip is higher.

Next, we derive the retraction speed at the tip of the liquid sheet. The constant volume assumption of the liquid sheet used in deriving Eq. (20) is not valid in this case. Indeed

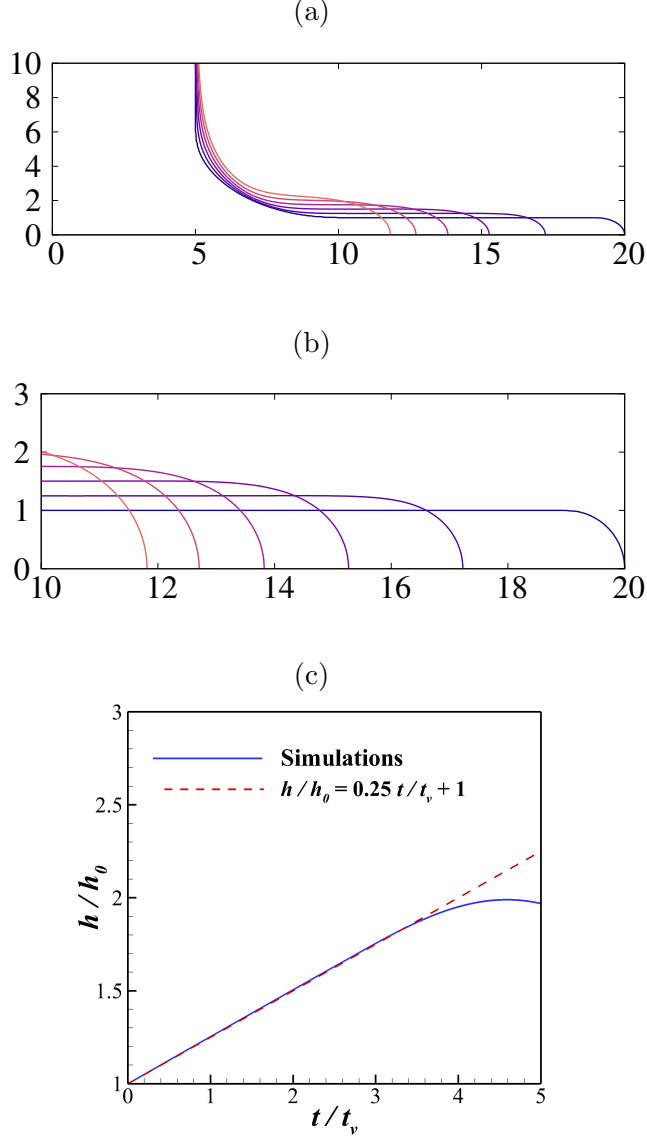


FIG. 5. (a) Interface profiles of the retracting sheet at different time instants. The profiles are shown at a time interval $\Delta t/t_v = 1$. (b) The zoomed view of the interface profiles is shown in (a). (c) Temporal variation of the thickness of the sheet at $x/h_0 = 10$. The dimensionless parameters are $Oh = 40$ and $L_0/h_0 = 10$.

the volume of the liquid sheet where the self-similar solution is valid (assumed to be the matching point between the circular arc and the 2D sheet) decreases continuously as the liquid drains out into the pool. Figure 7 (a) shows the **outflow** velocity at the end of the sheet ($x = 10h_0$) i.e. at the location where the sheet is connected to the large curvature region connecting to the pool. It is approximately equal to the viscous-capillary velocity γ/μ and decreases slowly as a function of time. Now considering that the end velocity is $u_e = \gamma/\mu$, we calculate the tip velocity of the retracting sheet. We include the outflow rate at the end of the sheet (up to which self-similar solution is valid) in the theoretical

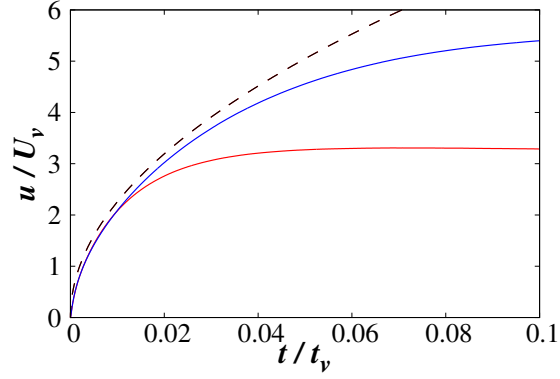


FIG. 6. Comparison of the retraction speed of the liquid sheet obtained from numerical simulations (solid lines) with the early stage retraction theory of Savva and Bush [14] (dashed line). The results are shown for $Oh = 40, L_0/h_0 = 10$ (red color) and $Oh = 40, L_0/h_0 = 20$ (blue color).

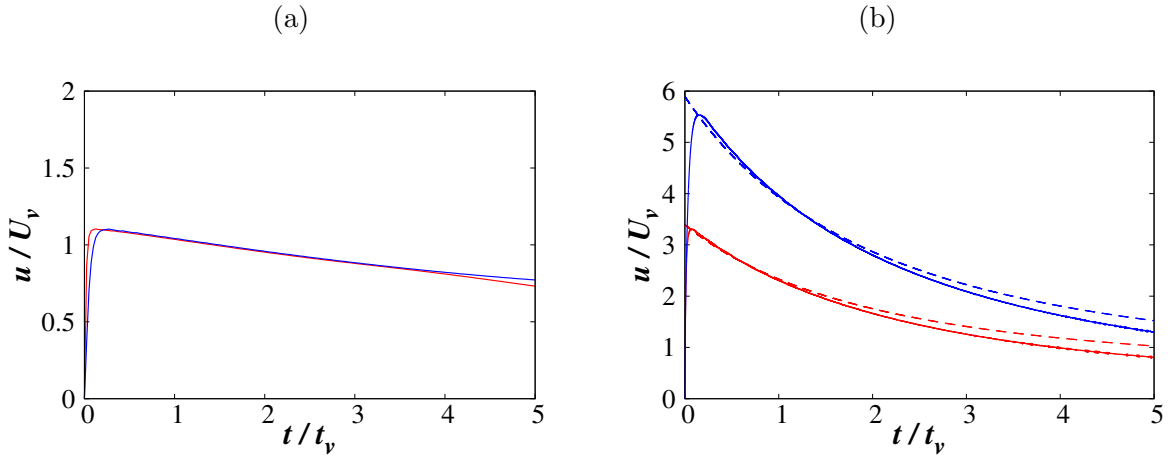


FIG. 7. (a) Velocity at the junction between the sheet and the initially circular arc ($x/h_0 = 10$). (b) Comparison of the retraction speed of the liquid sheet obtained from numerical simulations (solid lines) with the theoretical prediction of Eq. (23) (dashed line). The results are shown for $Oh = 40, L_0/h_0 = 10$ (red color) and $Oh = 40, L_0/h_0 = 20$ (blue color).

derivation. The volume of the portion liquid sheet (V) up to the connecting point to the pool after time t can be calculated as

$$V = V_0 - \int_0^t 2hu_e dt, \quad (21)$$

where V_0 is the initial volume of the liquid sheet. Now, assuming the tip of the liquid sheet to be semi-circular and considering the volume of the liquid sheet to be $V = (L - h)2h + \pi h^2/2$

we have

$$L = \frac{V_0}{2h} + h \left(1 - \frac{\pi}{4}\right) - \frac{1}{2h} \int_0^t 2hu_e dt \quad (22)$$

Now, using the similarity solution in a similar way [as described](#) in Sec. III A 1 we can find the tip speed as

$$\frac{dL}{dt} = U_v \left(-\frac{4(L_0/h_0 - 1) + \pi}{(t/t_v + 4)^2} + \frac{1}{4} \left(1 - \frac{\pi}{4}\right) - \frac{1}{2} - \frac{8}{(t/t_v + 4)^2} \right) \quad (23)$$

It is evident in Fig. 7 (b) that the numerical results are in reasonably good agreement with the theory. A deviation towards the later stage of retraction is a consequence of [two factors](#): first, the self-similar solution used in deriving Eq. (23) is not valid towards the later stage of retraction, and second, the assumed constant velocity at the end of the sheet decreases by a small amount in reality.

B. $Oh \sim L_0/h_0$

In this regime, the dimensional analysis of Sec. II A states that inertia and viscous effects are comparable. Therefore, a natural question that arises here is whether the similarity solution mentioned above is valid in this limit or not. Numerical simulations reveal that the thickness of the sheet increases linearly with time with a slope of 1/4 (not shown here) in good agreement with the self-similar solution.

Figure 8 shows the velocity of the tip in the short and long time limit for the two configurations discussed in the previous sections. The early-stage retraction theory of Savva and Bush [14] is in reasonable agreement with the numerical results (Figs. 8 (a) and (c)). A comparison of the retraction velocity of the sheet predicted by Eqs. (20) and (23) with the results obtained from the Basilisk simulations are shown in Figs. 8 (b) and (d) respectively. The models can predict the retraction speed with good accuracy. Even for the retraction in a pool, the theory is matching very well. This is because [the self-similar solution is valid and](#) the velocity at the end of the sheet is approximately equal to the assumed value ($u_e \approx \gamma/\mu$) for the entire period [considered here](#). Therefore we may conclude that even [though](#) the inertia and the viscous term are of the same order from a dimensional analysis point of view, it is apparent that the flow is dominated by the viscous effect.

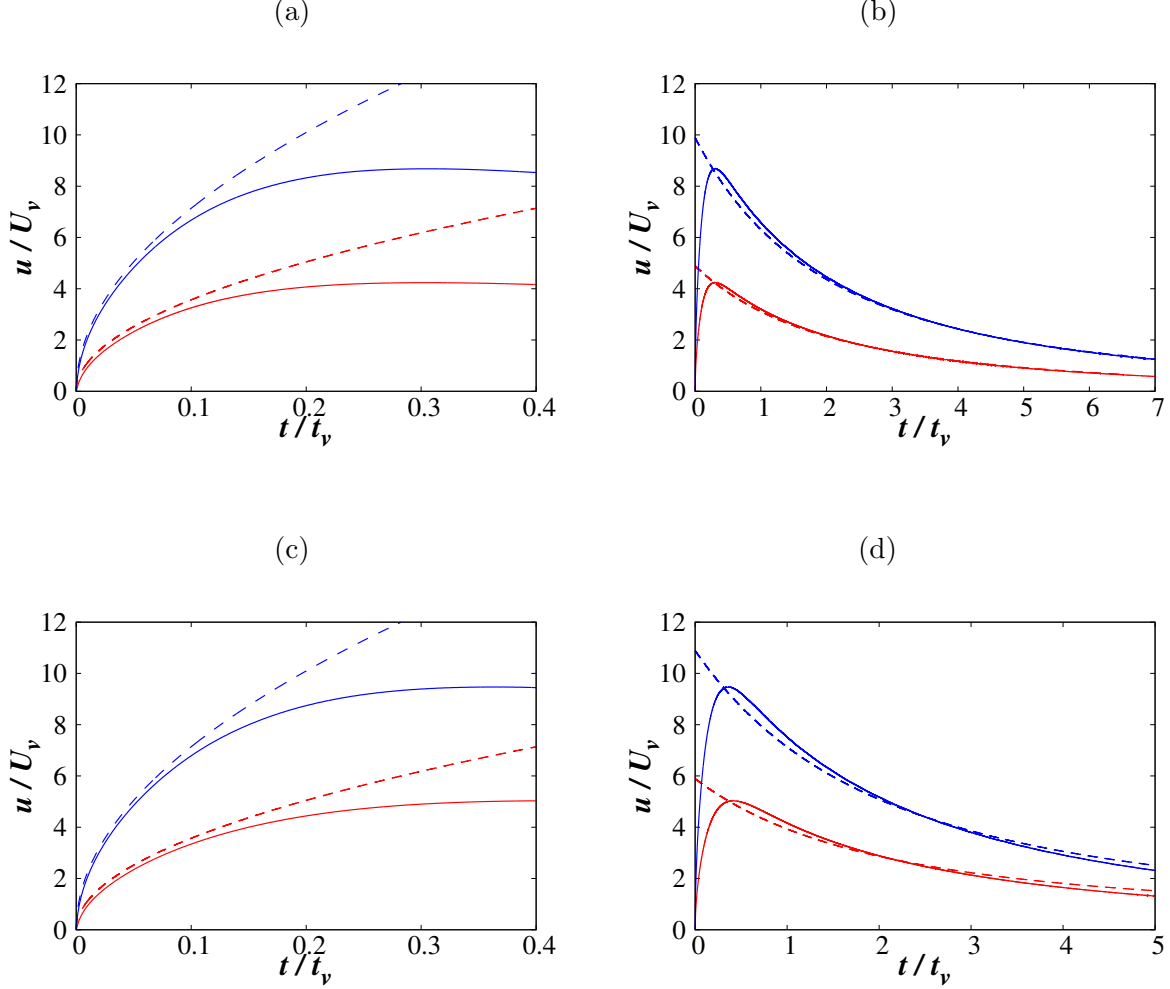


FIG. 8. Comparison of the retraction speed of the liquid sheet obtained from numerical simulations (solid lines) with the theoretical predictions (dashed lines) for the early stage (Savva and Bush [14]) and later stage (Eqs. (20) and (23)) of retraction. Here, (a) and (b) show the comparison of the numerical results and theory for the soap film (symmetric retraction) in the early stage and later stage of retraction respectively. (c) and (d) show the comparison of the numeric and theory in the early stage and later stage of retraction for the case of bursting bubble at the interface of a pool. The results are shown for $Oh = 20, L_0/h_0 = 20$ (red color) and $Oh = 40, L_0/h_0 = 40$ (blue color).

C. $Oh \ll L_0/h_0$

As the aspect ratio of the sheet increases, for a fixed Ohnesorge number, the inertia of the retracting sheet becomes non-negligible. Under such a condition, the sheet retracts with the formation of a bulbous end. Brenner and Gueyffier [17] proposed a [criterion](#) for the formation of the bulbous rim at the end in terms of Reynolds number (based on the length of the sheet and the Taylor-Culick speed) and Ohnesorge number. If we use the dimensionless parameters defined in the present article, their criterion for large Oh reads as

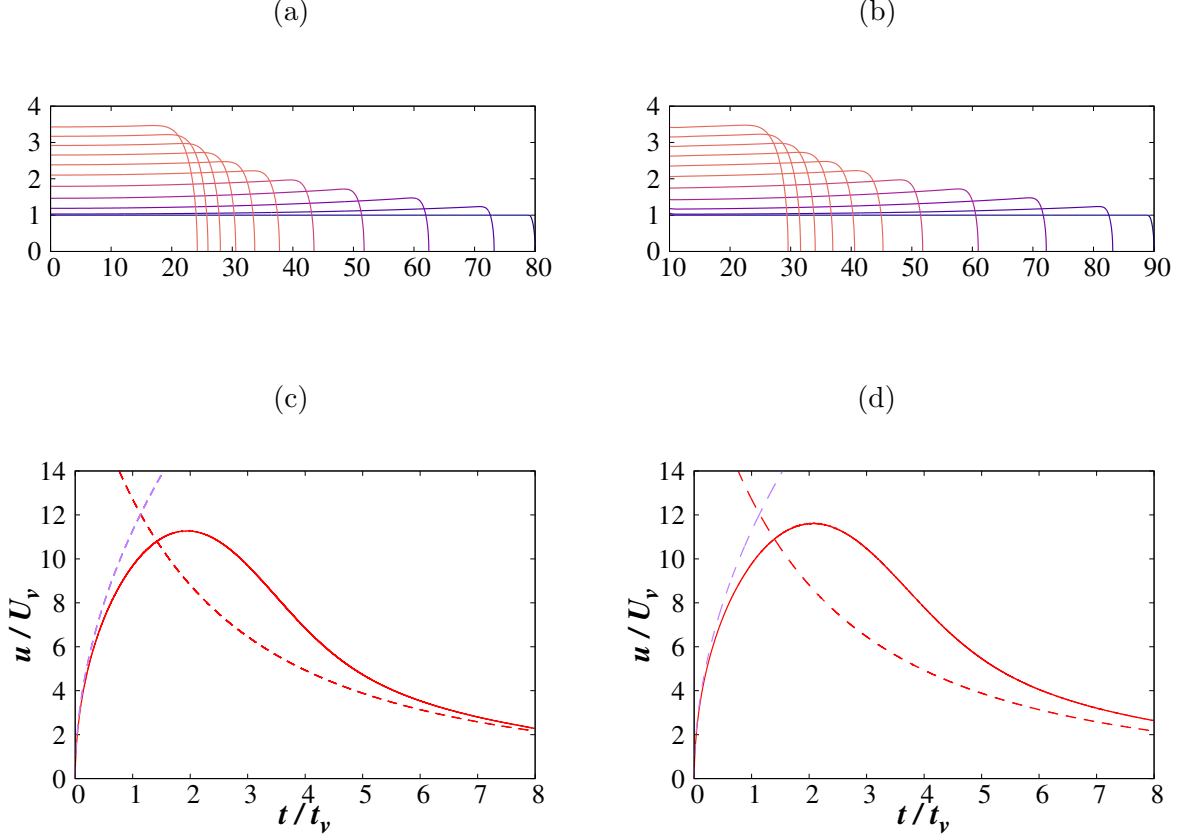


FIG. 9. Interface profiles at different time instants for the retraction of a symmetric film (a) and a bursting bubble at the liquid-air interface (b). The profiles are plotted at time interval $\Delta t/t_v = 1$ for $Oh = 20$ and $L_0/h_0 = 80$. A comparison of the retraction speed of the liquid sheet obtained from numerical simulations (solid lines) with the theoretical prediction (dashed lines) given by Eqs. (20) and (23) are shown in (c) and (d) respectively. The purple dashed line is the theoretical prediction of Savva and Bush [14] for the early stage of retraction.

$Oh > 1$ and $Oh > L_0/h_0$. Their criterion of viscous to inertial crossover is in agreement with the scaling analysis presented in Sec. II A. The Stokes flow assumptions are no longer valid for $Oh \ll L_0/h_0$. Under this condition, the liquid sheet retracts with the formation of a bulbous rim.

Figure 9 shows the interface profiles of a retracting soap film in (a) and a bursting bubble at the liquid-air interface in (b) along with the retraction speed in (c) and (d) respectively. The dimensionless parameters considered here are $Oh = 20$ and $L_0/h_0 = 80$. The self-similar solution becomes invalid in this regime and the sheet retracts with the formation of a small bulbous tip (see Fig. 9 (a) and (b)). In this limit, the retraction speed of the liquid sheet is not well predicted by the theory presented in Secs. III A 1 and III A 2 because the inertia effects are non-negligible. It can be observed in Figs. 9 (c) and (d) that the maximum speed

reached by the rim in these particular cases ($Oh = 20$ and $L_0/h_0 = 80$) is approximately $11U_v = 0.55U_{TC}$. We thus expect a value closer to the Taylor-Culick speed as the inertia effect increases.

IV. Discussion and concluding remarks

In the present work, we have studied the retraction of a liquid sheet of finite length in the large Oh limit where the viscous effect is dominant. Using the long-wavelength model we have derived the scaling laws as well as the similarity solution for the sheet profile in capillary-viscous dominated flow ($Oh \gg L_0/h_0$) where the sheet thickness increases uniformly across the whole domain. According to the self-similar solution, the sheet thickness grows linearly with time. Using the similarity solution we have derived the expression for the temporal variation of the retraction speed of the tip of the sheet. We have considered two configurations: the retraction of a soap film with a symmetric boundary condition at the extremity away from the tip, and, the retraction of the film of a bursting bubble at a liquid-air interface. The radius of curvature of the liquid films is considered to be large enough to have negligible effects on the retraction dynamics. We have shown that in both configurations, the retraction speed of the sheet decreases as the inverse-square of time which is in agreement with the numerical results when the inertia effect is not significant i.e. for $Oh \gg L_0/h_0$ and $Oh \sim L_0/h_0$.

Sünderhauf *et al.* [6] and Savva and Bush [14] have shown that even when the viscous effect is important, the tip of a retracting sheet always reaches the Taylor-Culick speed. However, why is the speed reached in the present study in the high Oh limit so different from the Taylor-Culick speed? The major difference between the present study and the studies of Refs. [6] and [14] is that they considered a pseudo infinite sheet by writing the equations in a frame moving with the tip. The scaling analysis performed here shows that the inertia effect can not be neglected even for high Ohnesorge number if the aspect ratio is sufficiently high ($Oh \ll L_0/h_0$). In the present investigation, the sheet has a finite aspect ratio. The reduction of the rim speed of a finite sheet may be attributed to viscous effects. In the long time limit, the two opposing ends of the sheet retract towards each other to form a stationary liquid cylinder (soap film configuration) or the liquid film retracts towards a stationary pool to completely coalesce into it (bursting bubble configuration). The capillary pressure difference near the tip created by the change in curvature drives the flow which

is resisted by the viscosity of the liquid. The capillary pressure difference decreases with time as the sheet thickness increases (uniformly) resulting in a decrease in the driving force, while the viscous resistance acts continuously. In contrast, for a semi-infinite sheet and finite Oh , the film thickness increases near the tip and gradually decreases further away from the tip. The region of influence of the tip motion is proportional to Oh [14] and a uniform increase in the whole film thickness is not a valid assumption for $Oh \ll L_0/h_0$. For an infinite sheet, the maximum thickness of the sheet increases linearly with time (as observed by Savva and Bush [14] for high Oh) not the thickness in the far-field. Because of this reason a decreasing speed is not witnessed in Refs. [6] and [14] in the long time limit. Moreover, due to the absence of edge effects, the retraction speed of the sheet continues increasing until there is a balance between the capillary force and the inertia, and hence reaches the Taylor-Culick speed. However, this does not imply that viscous dissipation does not play any role in the retraction process of a semi-infinite sheet. Indeed, half of the surface energy is dissipated through viscous dissipation and the other half is converted to kinetic energy as demonstrated numerically and theoretically in Ref. [6] and Ref. [14] respectively. Here, the viscous effect merely affect how momentum is distributed in the sheet but does not affect the final retraction speed in the long time limit. This explains why Taylor-Culick speed is achieved even for high Oh in Refs. [6] and [14].

Next, it is a natural intuition to know about the evidence of the decrease in the retraction speed in the experiments. Considering the bubble bursting at the free surface of water (tap water or seawater), as reported in Lhuissier and Villermaux [29], the typical value of the Ohnesorge number is less than 1 while the aspect ratio is approximatively 10000. Thus inertia plays an important role in the retraction of the film and as a result, the Taylor-Culick velocity is reached. The retraction dynamics in those configurations are different from the present study which is focused on the high Oh limit. The present analysis applies to the bubble bursting at the free surface of a highly viscous liquid, for instance, in glass furnaces or during volcanic eruptions. Debrégeas *et al.* [30] studied experimentally the bursting kinetics of an air bubble rising at the free surface of a highly viscous (and viscoelastic) liquid. The typical dimensionless parameters in their experiments were: $Oh \approx 10^5$ and $L_0/h_0 \approx 10000$, a range of value in agreement with the present theory. In figure 2 (b) of their paper, they evidenced the decrease of the retraction speed in the later stage of the retraction process. The authors explained this singular behaviour by the fact that the rim was meeting progressively

thicker film, i.e. the film thickness was non-uniform. It is rather questionable whether the decrease of the rim velocity can be explained by the present theory or by the argument provided by Debrégeas *et al.* [30] and a detailed study is needed to disentangle both effects. Also in the present study, we have assumed that the liquid surface is clean and the system is isothermal. This is far from being the case in many experiments where surfactant can be present. For instance, in the experiments of Lhuissier and Villermaux [29] surfactants are naturally present since tap water is used for the liquid phase. However, no effect of the surfactants on the retraction velocity was seen since the rim reached the Taylor-Culick velocity. On the other hand, the recent investigation of Constante-Amores *et al.* [31] on the retraction of liquid ligaments suggests that the presence of surfactants and the reduction in surface tension lead to a reduction of the retraction velocity. Their analysis was performed in the inertia dominated regime (low Oh) and for a liquid ligament. De Malmazet *et al.* [32] studied the coalescence of drop at liquid-liquid interface in presence of micro-particles. They observed that the retracting sheet bend due to the difference of interfacial tension on both sides of the sheet. Hence, the presence of the surfactants or presence of temperature gradient may change the present results which need further investigation.

V. Acknowledgements

Financial support of IFP Energies Nouvelles is gratefully acknowledged.

-
- [1] E. Villermaux and C. Clanet, Life of a flapping liquid sheet, *Journal of Fluid Mechanics* **462**, 341 (2002).
 - [2] N. Bremond, C. Clanet, and E. Villermaux, Atomization of undulating liquid sheets, *Journal of Fluid Mechanics* **585**, 421 (2007).
 - [3] J. Eggers and E. Villermaux, Physics of liquid jets, *Reports on Progress in Physics* **71**, 036601 (2008).
 - [4] X. Hu and A. M. Jacobi, The Intertube Falling Film: Part 1 – Flow Characteristics, Mode Transitions, and Hysteresis, *Journal of Heat Transfer* **118**, 616 (1996).
 - [5] D. S. Finnicum, S. J. Weinstein, and K. J. Ruschak, The effect of applied pressure on the shape of a two-dimensional liquid curtain falling under the influence of gravity, *Journal of Fluid Mechanics* **255**, 647 (1993).

- [6] G. Sünderhauf, H. Raszillier, and F. Durst, The retraction of the edge of a planar liquid sheet, *Physics of Fluids* **14**, 198 (2002).
- [7] A. Dupré, Sixième memoire sur la theorie mécanique de la chaleu, *Ann. Chim. Phys.* **4**, 194 (1867).
- [8] W. E. Ranz, Some experiments on the dynamics of liquid films, *Journal of Applied Physics* **30**, 1950 (1959).
- [9] G. I. Taylor, The dynamics of thin sheets of fluid. III. Disintegration of fluid sheets, *Proceedings of the Royal Society of London. Series A. Mathematical and Physical Sciences* **253**, 313 (1959).
- [10] F. E. C. Culick, Comments on a ruptured soap film, *Journal of Applied Physics* **31**, 1128 (1960).
- [11] W. R. McEntee and K. J. Mysels, Bursting of soap films. I. An experimental study, *The Journal of Physical Chemistry* **73**, 3018 (1969).
- [12] J. B. Keller, Breaking of liquid films and threads, *The Physics of Fluids* **26**, 3451 (1983).
- [13] A. B. Pandit and J. F. Davidson, Hydrodynamics of the rupture of thin liquid films, *Journal of Fluid Mechanics* **212**, 11 (1990).
- [14] N. Savva and J. W. M. Bush, Viscous sheet retraction, *Journal of Fluid Mechanics* **626**, 211 (2009).
- [15] L. Gordillo, G. Agbaglah, L. Duchemin, and C. Josserand, Asymptotic behavior of a retracting two-dimensional fluid sheet, *Physics of Fluids* **23**, 122101 (2011).
- [16] M. Murano and K. Okumura, Bursting dynamics of viscous film without circular symmetry: The effect of confinement, *Physical Review Fluids* **3**, 031601 (2018).
- [17] M. P. Brenner and D. Gueyffier, On the bursting of viscous films, *Physics of Fluids* **11**, 737 (1999).
- [18] J.-L. Pierson, J. Magnaudet, E. J. Soares, and S. Popinet, Revisiting the taylor-culick approximation. retraction of an axisymmetric filament (in press), *Physical Review Fluids* (2020).
- [19] T. Erneux and S. H. Davis, Nonlinear rupture of free films, *Physics of Fluids A: Fluid Dynamics* **5**, 1117 (1993).
- [20] A. Oron, S. H. Davis, and S. G. Bankoff, Long-scale evolution of thin liquid films, *Reviews of Modern Physics* **69**, 931 (1997).

- [21] G. I. Barenblatt and B. G. Isaakovich, *Scaling, self-similarity and intermediate asymptotics: dimensional analysis and intermediate asymptotics*, Vol. 14 (Cambridge University Press, 1996).
- [22] J. Eggers, Post-breakup solutions of Navier-Stokes and Stokes threads, *Physics of Fluids* **26**, 072104 (2014).
- [23] J. P. Munro and J. R. Lister, Capillary retraction of the edge of a stretched viscous sheet, *Journal of Fluid Mechanics* **844**, R1 (2018).
- [24] J. Eggers and M. A. Fontelos, *Singularities: Formation, Structure, and Propagation* (Cambridge University Press, Cambridge, UK, 2015) pp. 1–453.
- [25] S. Popinet, An accurate adaptive solver for surface-tension-driven interfacial flows, *Journal of Computational Physics* **228**, 5838 (2009).
- [26] S. Popinet, A quadtree-adaptive multigrid solver for the Serre-Green-Naghdi equations, *Journal of Computational Physics* **302**, 336 (2015).
- [27] Basilisk, <http://basilisk.fr>.
- [28] H. Deka, J.-L. Pierson, and E. J. Soares, Retraction of a viscoplastic liquid sheet, *Journal of Non-Newtonian Fluid Mechanics* **272**, 104172 (2019).
- [29] H. Lhuissier and E. Villermaux, Bursting bubble aerosols, *Journal of Fluid Mechanics* **696**, 5 (2012).
- [30] G. Debrégeas, P.-G. de Gennes, and F. Brochard-Wyart, The life and death of “bare” viscous bubbles, *Science* **279**, 1704 (1998), <https://science.sciencemag.org/content/279/5357/1704.full.pdf>.
- [31] C. R. Constante-Amores, L. Kahouadji, A. Batchvarov, S. Shin, J. Chergui, D. Juric, and O. K. Matar, Dynamics of a surfactant-laden bubble bursting through an interface, arXiv preprint arXiv:2005.04472 (2020).
- [32] E. De Malmazet, F. Risso, O. Masbernat, and V. Pauchard, Coalescence of contaminated water drops at an oil/water interface: Influence of micro-particles, *Colloids and Surfaces A: Physicochemical and Engineering Aspects* **482**, 514 (2015).